Journal of Ultrafine Grained and Nanostructured Materials
https://jufgnsm.ut.ac.ir
Vol. 58, No.2, June 2025, pp. 219-227
Print ISSN: 2423-6845 Online ISSN: 2423-6837
DOI: 10.22059/jufgnsm.2025.02.07

Enhanced Stability of Perovskite Solar Cells through MACl-Induced Crystallinity Improvement and Suppression of Ion Migration

Zhila Khakpour[a,b], Omran Moradlou[a,c]*, Hanieh Sharifian[b], Maryam Heidariramsheh[d]*, Nima Taghavinia[b,e]*

[a]Department of Analytical Chemistry, Faculty of Chemistry, Alzahra University, Tehran, Iran
[b]Nanoparticles and Coatings Lab, Department of Physics, Sharif University of Technology, Tehran, Iran
[c]Institute of Atomic and Molecular Sciences, Academia Sinica, Taipei 10617, Taiwan
[d]School of Metallurgy and Materials Engineering, College of Engineering, University of Tehran, Tehran, Iran
[e]Center for Nanoscience and Nanotechnology, Sharif University of Technology, Tehran, Iran

Recieved: 2 July 2025; Accepted: 26 August 2025

[*]Corresponding authors, E-mail: moradlou@alzahra.ac.ir, m.heidariramsheh@ut.ac.ir, taghavinia@sharif.edu

ABSTRACT

Addressing challenges related to the structural defects, ion migration, and instability in perovskite solar cells, this study investigates the impact of incorporating methylammonium chloride (MACl) into the perovskite precursor solution. The optimal addition of MACl (10 mg/mL) resulted in perovskite films with grain growth improvement and fewer grain boundaries, as observed by field emission scanning electron microscopy. Furthermore, X-ray diffraction analysis showed an increased preferential orientation along the (001) and (002) crystal planes, while UV-Vis and photoluminescence spectroscopy data indicated smooth surface and reduced defects induced recombination. Consequently, the fabricated PSCs with the optimized composition achieved a power conversion efficiency of 14.56%, representing a significant improvement over the control device (12.81%) and the sample with excess MACl (20 mg/mL, 13.43%). This enhanced performance was attributed to improvements in all photovoltaic parameters, along with a notable reduction in the hysteresis index, indicating suppressed ion migration. Electrochemical impedance spectroscopy analysis further supported these improvements by revealing reduced charge transfer resistance and enhanced recombination resistance. Importantly, the optimized devices demonstrated enhanced power output, retaining 85% of their initial performance after 120 s light soaking. These results indicate that optimized MACl incorporation is an effective strategy for simultaneously improving the efficiency and stability of PSCs by enhancing crystallinity, suppressing ion migration, and promoting defect passivation.

Keywords: *Perovskite solar cell, methylammonium chloride, hysteresis, ion migration, crystallinity.*

1. Introduction

In recent years, the growing global energy demand and the challenges associated with fossil fuels have significantly increased interest in renewable energies [1-3]. Among these, perovskite solar cells (PSCs), have become one of the main candidates to replace silicon solar cells due to their unique advantages such as low manufacturing cost, solution processing capability, and photon-to-electricity conversion efficiency of more than 26% in a short period of time after their emergence [4-6]. Despite the high efficiency, challenges such as long-term stability and hysteresis behavior in current-voltage response are the main obstacles to the commercialization of this generation of solar cells. The hysteresis phenomenon in the current density-voltage (J-V) curve is characterized by the difference in cell performance in the forward and reverse direction of voltage scan. Hysteresis not only causes the non-reproducibility of PSC performance but also hinders the standardization of measurements and is also an indication of poor stability under long-term operating conditions [7].

Several studies have been conducted to investigate the causes of hysteresis and ion migration. In particular, migration of methylammonium (MA^+) and iodide (I^-) ions has been identified as an important factor. Under the influence of an external electric field or internal field, these ions are able to migrate into the perovskite absorber layer through the structural defects and accumulate at the perovskite interface with the charge-transporting layers. This accumulation leads to the formation of charged regions and an increase in non-radiative recombination of charge carriers [8,9]. In addition to increasing hysteresis, this phenomenon also reduces the long-term stability of the cell. Consequently, controlling and reducing ion migration is recognized as a key strategy for improving the performance of PSCs [10].

One of the most effective methods is to improve the crystallinity of the perovskite film and reduce its associated defects, because the more regular the crystal structure of the perovskite layer and the fewer the grain boundaries, the more restricted the ion migration path and the more stable the PSC performance. Improving crystallinity also reduces recombination centers, increases the lifetime of charge carriers, and ultimately improves photovoltaic performance [11].

Adding additives such as MACl to the perovskite precursor solution is a simple and controllable method to improve the crystallinity of perovskite films. MACl provides suitable conditions for better crystal orientation and more homogeneous grain growth and plays an effective role in engineering the perovskite layer structure and reducing ion migration, thereby reducing hysteresis [12]. Also, the presence of chloride in the early stages of crystallization may reduce electronic defects and improve the surface quality of the film and have a positive effect on the deposition of the hole transport layer. All of these factors have a direct effect on reducing hysteresis and increasing the long-term stability of PSCs [13]. However, this additive has often been used in simple perovskite compositions ($FAPbI_3$ and $CsFAPbI_3$) [14].

In this study, MACl was added to the triple cation perovskite precursor solution at different concentrations of 0, 10, and 20 mg/mL to investigate its effect on the crystallinity, morphology, optical, and photoelectronic properties of the perovskite film. The main goal of this study is to understand the relationship between improved crystallinity, perovskite layer quality, and reduced ion migration, reduced hysteresis, and ultimately the enhancement of both efficiency and operational stability in PSCs.

2. Experimental Details

PSCs with the structure FTO/c-TiO_2/m-TiO_2/PSK/CIS/C were fabricated on pre-patterned Fluorine-doped Tin Oxide (FTO) coated glass substrates (1.4×1.4 cm^2). The FTO substrates were sequentially cleaned by ultrasonicating for 20 minutes in soapy water, isopropyl alcohol, ethanol, and deionized water. The substrates were then dried under a stream of dry air.

2.1. Compact TiO_2 (c-TiO_2) Deposition

A compact TiO_2 layer was deposited by spin-coating. The precursor solution was prepared by first dissolving 0.357 g of titanium (IV) isopropoxide (TTIP) in 1.999 g of ethanol (Solution A) inside a glovebox. Separately, 0.042 g of hydrochloric acid (HCl) was dissolved in 1.999 g of ethanol (Solution B). Solution B was then added dropwise to Solution A, and the resulting solution was filtered through a 0.22 μm filter. Prior to deposition, the FTO substrates were treated with UV-ozone for 30 minutes. Next, 200 μL of the filtered precursor solution was spin-coated onto the FTO substrate at 2000 rpm for 30 seconds. Immediately after spin-coating, the edges of the substrate were cleaned with ethanol, and the films were finally sintered at 500 °C for 30 minutes in air.

2.2. Mesoporous TiO_2 (m-TiO_2) Deposition

A mesoporous TiO_2 layer was deposited by spin-coating a diluted commercial TiO_2 paste. The paste was diluted with absolute ethanol at a weight ratio of 5.5:1 and stirred magnetically for 24 hours. The FTO/c-TiO_2 substrates were treated with UV-ozone for 20 minutes prior to deposition. Then, 70 μL of the diluted TiO_2 solution was spin-coated onto the FTO/c-TiO_2 substrate at 4000 rpm for 30 seconds. The edges were then cleaned with ethanol, and the films were sintered at 500 °C for 30 minutes in air.

2.3. Perovskite Absorber Layer Deposition

The triple-cation perovskite solution, $Cs_{0.05}(FA_{0.83}MA_{0.17})_{0.95}Pb(I_{0.83}Br_{0.17})_3$, was prepared inside a nitrogen-filled glovebox by dissolving 0.5486 g of PbI_2, 0.0571 g of $PbBr_2$, 0.1789 g of formamidinium iodide (FAI), 0.0174 g of methylammonium bromide (MABr), 0.0270 g of cesium iodide (CsI), and in varying amounts of methylammonium chloride (MACl) (0.0 g, 0.01 g, and 0.02 g) in 1 mL of a dimethylformamide (DMF):dimethyl sulfoxide (DMSO) mixture (1:4 by volume). The solution was stirred magnetically for 30 minutes. Before deposition, the FTO/c-TiO_2/m-TiO_2 substrates were treated with UV-ozone for 30 minutes. The perovskite film was deposited using a two-step spin-coating program at 1000 rpm for 10 seconds, followed by 6000 rpm for 30 seconds inside the glovebox. During the last 10 seconds of the second spin-coating step, 270 μL of chlorobenzene was rapidly dispensed as an antisolvent. The resulting films were then annealed

on a hot plate at 100 °C for 1 hour inside the dry box. To refer the samples based on the amount of MACl additive, we define three sample code including MACl-0, MACl-10, and MACl-20.

2.4. Hole Transport Layer (CIS) Deposition

The hole transport layer was deposited by spin-coating a commercial CIS solution. 80 µL of the CIS solution was spin-coated at 3000 rpm for 30 seconds. This process was repeated once to increase the layer thickness. Following the deposition, the samples were annealed at 100 °C for 10 minutes on a hot plate.

2.5. Carbon Back Electrode Deposition

A carbon back electrode was deposited using the Doctor Blade method. Immediately after deposition, the devices were dried in an oven at 100 °C for 30 minutes.

2.6. Characterization

X-ray diffraction (XRD) patterns were obtained using a PANalytical, X'Pert Pro MPD X-ray diffractometer with Cu Kα radiation (λ = 1.5406 Å). The surface topography image of layers were investigated using the field-emission scanning electron microscopy (FESEM, TESCAN, Mira 3-XMU). The steady-state photoluminescence spectra were recorded by Avantes TEC-2048 spectrometer using the diode laser (λ = 405 nm), while the illumination and photon collection was from the glass side. The ultraviolet–visible (UV–vis) absorption/transmission spectra were recorded with a PerkinElmer Lambda 25 spectrophotometer equipment. A solar simulator (IRASOL SIM- 1020 system) with an AM 1.5G filter was used to provide 100 mW cm^{-2} of illumination on the solar cells, with the intensity calibration using a Si photodiode. The J-V characteristics were obtained using the Palmsens potentiostat source meter. The voltage sweep was performed from 1.2 V to -0.01 V (reverse scan), and back from -0.01 V to 1.2 V (forward scan), both at the same scan rate of 5 mV s^{-1}. The Stabilized Power Output (SPO) analysis was performed under standard irradiance of AM 1.5G illumination and at the maximum power point voltage for 120 seconds using the Palmsens potentiostat source meter. Incident photon-to-current efficiency (IPCE) was measured by IPCE-020 IRASOL instrument under short-circuit conditions. Impedance spectra were recorded to measure charge transfer resistance and recombination resistance. This analysis was performed by potentiostat galvanostat-PGE 18 (IRASOL) and a white LED light source (to prevent warming).

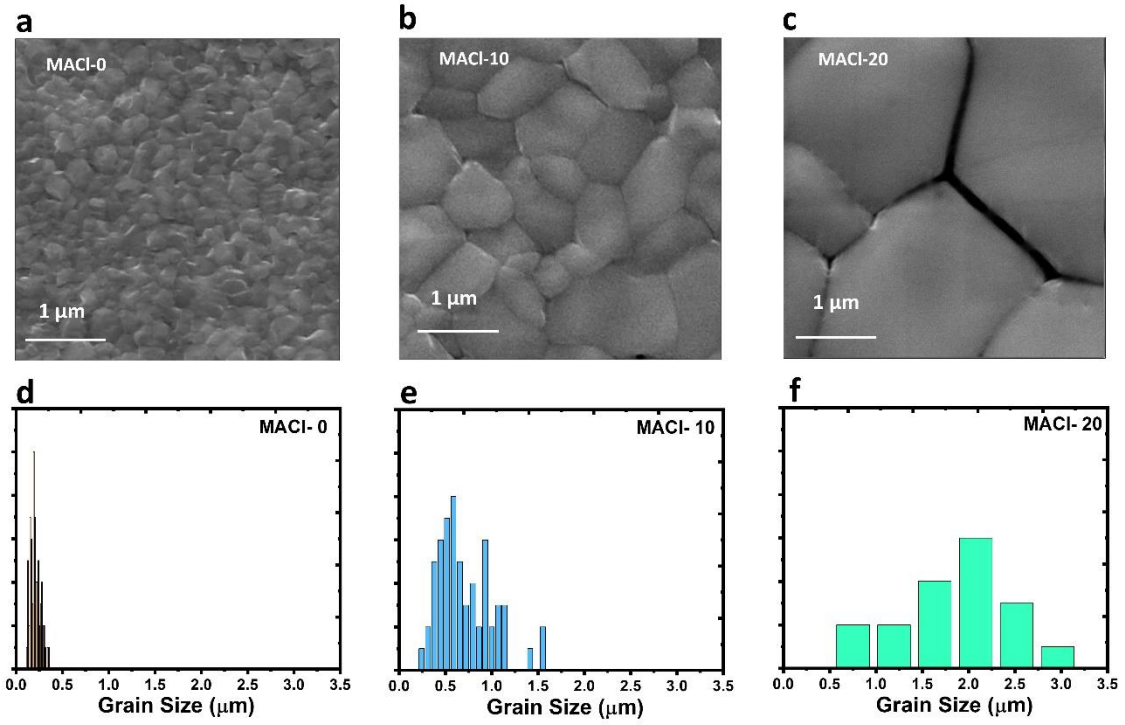

Fig. 1- Top-view FE-SEM images of perovskite films prepared with different concentrations of MACl: (a) 0 mg/mL (MACl-0), (b) 10 mg/mL (MACl-10), and (c) 20 mg/mL (MACl-20). Grain size distributions derived from the corresponding FE-SEM images are shown in (d) MACl-0, (e) MACl-10, and (f) MACl-20.

3. Result and discussion

Figure 1 a–c show the FE-SEM images of the top surface of the perovskite layer with different MACl concentrations (10 and 20 mg/mL) in comparison with MACl free layer, at a magnification of 25 kx. As it is clear, the addition of MACl to the perovskite precursor solution led to a significant increase in the grain size of the perovskite layer. Based on the analysis with the appropriate software (Image J), the average grain sizes shown in Figure 1d-f, for the samples without MACl, with 10, and 20 mg/mL MACl were estimated to be 0.2, 0.7, and 1.8 μm, respectively. It is expected that the increase in grain size leads to a decrease in the density of defects at the grain boundaries, which results in improved charge carrier lifetime by decrease in the recombination rate of charge carriers. This effect is especially pronounced in the MACl-10 sample. However, in the MACl-20 sample, although the grain size increase significantly, voids are observed between the grains. This phenomenon can lead to the formation of discontinuities in the charge transport path, an increase in the density of boundary defects, and ultimately an increase in the electron-hole recombination rate. As a result, the photovoltaic performance may be reduced under these conditions [15].

Figure 2a compares the XRD patterns related to the additive-free perovskite samples (MACl-0) and the MACl-10 sample. A significant change of growth mode is observed [16]. The corresponding Williamson-hall diagram was extracted from XRD patterns (Figure 2b). The crystallite size was calculated to be 53 and 91 nm for MACl-0 and MACl-10 respectively. Furthermore, Figure 2c shows the amount of Full Width at Half Maximum (FWHM) and texture coefficient for MACl-0 and MACl-10. Regarding the MACl-0 sample, the diffraction pattern indicates the random growth of crystals without any significant preferential growth along the crystalline planes. In contrast, the MACl-10 sample shows a significant increase in the intensity of the peaks corresponding to the (001) and (002) planes, indicating the preferential orientation of crystal growth in these planes [1]. The preferential orientation on (001) and (002) planes can lead to improved charge transport in the perovskite layer, as these planes provide more direct paths for charge carrier movement and reduce non-radiative recombination. Furthermore, in both samples, the peaks corresponding to the PbI_2 phase are not observed, indicating the complete inclusion of the lead precursors to the perovskite structure. A decrease in the FWHM value is observed for all the diffraction peaks, particularly for the (001), (112), and (222) planes [16].

Figure 2d shows the photoluminescence (PL) spectra of perovskite films containing different amounts of MACl. With the addition of 10 mg/mL MACl, the PL peak intensity increases significantly, indicating an improvement in crystallinity and a decrease in non-radiative recombination centers. This is consistent with the data obtained from FESEM images and XRD patterns. However, at a concentration of 20 mg/mL, the PL intensity decreases, likely due to an increase in structural defects in the grain boundaries and the presence of voids between them [17].

A notable point in the PL spectra is the observation of a shift of the photoluminescence peak to higher photon energies (blue shift) with increasing MACl content. This shift may be due to structural changes and local strains in the perovskite film, which occur as a result of the improvement of crystal growth and film quality due to the presence of MACl. These findings are consistent with recent reports, such as Zhang et al., which showed that the addition of MACl can not only improve crystallinity but also change the optoelectronic properties and energy bandgap of perovskite films [18,19]. In other words, the incomplete removal of MACl during perovskite annealing, along with the residual methyl ammonium and chlorine in the final perovskite composition, can lead to an increase in the band gap.

The optical absorption of the perovskite films was investigated using UV–Vis spectroscopy (Figure 2e). The results showed that adding 10 mg of MACl to the perovskite precursor solution caused the absorption edge of the perovskite film to become sharper and shift towards higher energies (blue shift). This behavior indicates enhanced crystallinity and reduced defect density, which is also consistent with the increased intensity of the photoluminescence peak. In contrast, for the MACl-20 sample, the absorption edge became less sharp and the absorption intensity decreased, possibly due to unpacked microstructure. Additionally, similar to the PL results, a shift towards higher energies was observed in the UV–Vis spectrum of the MACl-20 sample [1, 20-22].

The fabricated solar cells have the FTO/c-TiO_2/m-TiO_2/PSK/CIS/C configuration (Figure 3a). To evaluate the photovoltaic performance of the devices with perovskite absorber layers containing different amounts of MACl additive, the J–V measurement was performed under simulated AM 1.5G irradiation in both forward and reverse scan directions, using a potential sweep rate of 100 mV s^{-1} (Figure 3b). The calculated photovoltaic parameters were summarized in Table 1. The results showed that the addition of MACl had a significant impact on the final performance of the devices, with the efficiency increasing from 12.81% for the MACl-0 sample to 14.56% in the MACl-10 sample, then decreasing to 13.43% at a higher

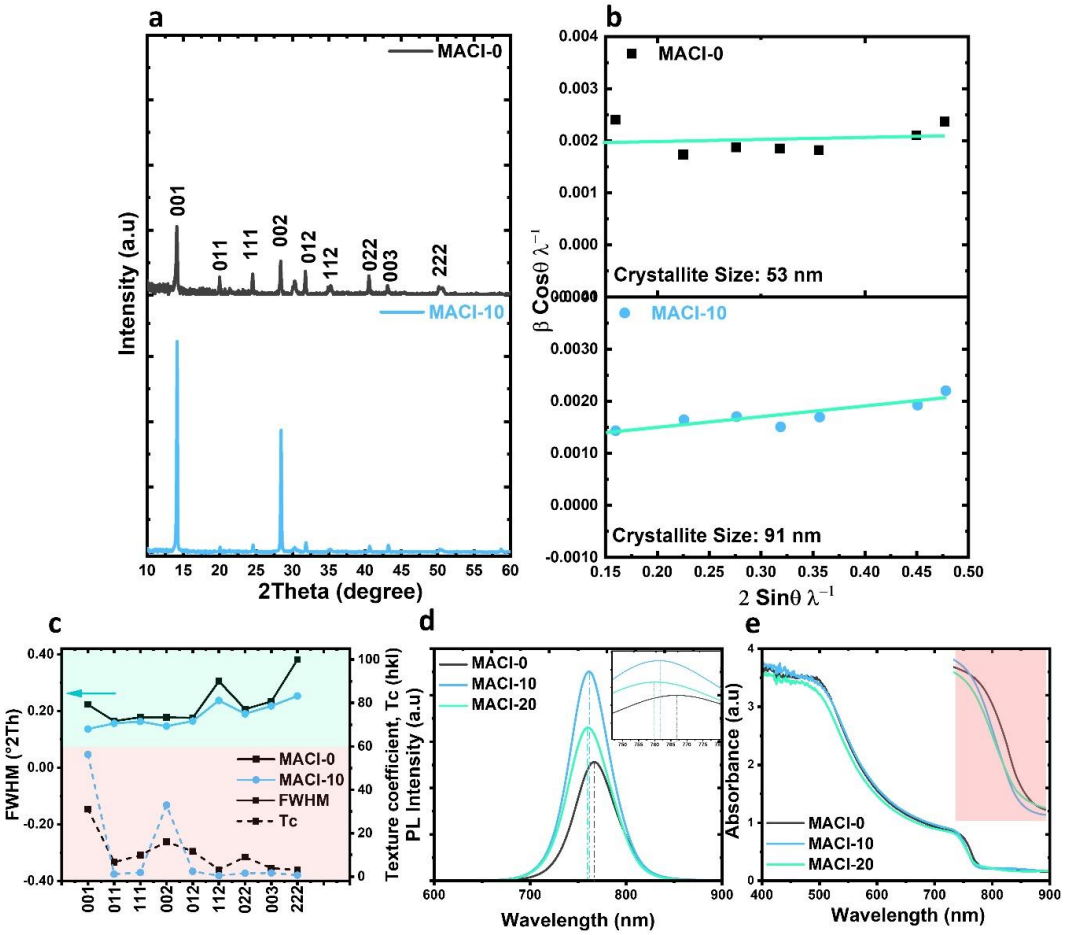

Fig. 2- (a) XRD patterns of perovskite films containing 0 and 10 mg/mL MACl; (b) corresponding Williamson–Hall plots illustrating crystallite size; (c) texture coefficient and FWHM values; (d) PL spectra measured from the glass side using a diode laser (λ = 405 nm); and (e) UV–vis absorbance spectra of MACl-0, MACl-10, and MACl-20.

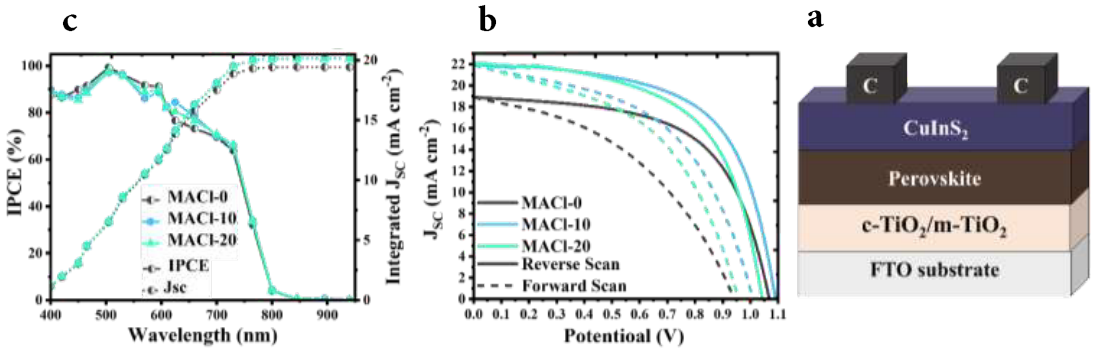

Fig. 3- (a) Schematic illustration of the device structure; (b) J–V curves of the champion PSCs measured under AM 1.5G illumination from +1.2 V to -0.01 V (reverse scan), and back from -0.01 V to +1.2 V (forward scan), both at the same scan rate of 5 mV s^{-1}; and (c) IPCE spectra of PSCs fabricated with different concentrations of MACl (0, 10, and 20 mg/mL).

concentration of MACl (MACl-20). These changes are mainly due to the improvement of open circuit voltage (V_{OC}) and short circuit current density (J_{SC}) in the MACl-10 sample and the decrease in these parameters, especially fill factor (FF), in the MACl-20 sample. The efficiency enhancement observed in the MACl-10 sample can be directly correlated with structural and optical analysis results. The larger grain size and higher film density, along with the improved crystal orientation and reduced structural defects, contribute to more efficient charge transport.

IPCE results showed that the samples containing MACl exhibited higher quantum efficiency in the red spectral region compared to the control sample (Figure 3c). This enhanced optical response is attributed to improved crystallinity and the overall quality of the perovskite layer. Improved crystallinity reduces recombination centers and increases the charge carrier lifetime, thereby leading to enhanced photon-to-electrical current conversion, particularly in the red spectral region (600-700 nm).

We also applied the proposed approach to 6 additional devices fabricated under the same experimental conditions. Statistical analysis of the J–V parameters for these 6 cells (Fig. 4a–d) further confirmed that the addition of 10mg/ml MACl improved all photovoltaic parameters. A Comparison series (R_{Series}) and shunt (R_{Shunt}) resistance (Fig. 4e and f) showed that the decrease in R_{Series} and the increase in R_{Shunt} in the MACl-10 sample were the main factors contributing to the enhanced fill factor (FF), while the opposite trend was observed in the MACl-20 sample.

One of the noteworthy findings of this study is the significant decrease in the hysteresis index (HI) observed in the samples containing MACl, particularly in the MACl-10 sample (Figure 5a). The HI in this sample is nearly half that the MACl-0 sample, indicating a significant suppression of hysteresis with the optimal amount of MACl. Since the ion migration is one of the primary causes of the hysteresis in PSCs, and given the improvement in crystal quality and film uniformity, the decrease in HI can be attributed to the likely decrease in the migration of mobile ions such as MA^+ or I^-. However, the exact mechanism requires further investigation [23-26].

In order to evaluate the stability of solar cells under real working conditions, the SPO analysis was performed under standard irradiance of 1 sun and at the maximum power point voltage for 120 seconds. As shown in Figure 5b, the MACl-10 sample exhibited the highest stability, maintaining 85% of its initial current density after 120 s. In contrast, the MACl-20 sample showed a sharp decrease in output power, with only about 25% of the initial current remaining at the end of the test. This performance aligns well with the trends observed in previous results. Since ion migration is a key factor contributing to the performance instability of PSCs in SPO analysis, the suppression of this phenomenon has played an effective role in maintaining stable performance observed in the MACl-10 sample. In contrast, the MACl-20 sample which exhibited the sharp drop in photovoltaic performance, the increase in series resistance, and the decrease in shunt resistance, suggests that the unpacked microstructure and poor grain, causes the activation of ion migration channels and rapid recombination, ultimately leading to a sharp drop in stability in the SPO test [27,28].

Table. 1- Photovoltaic parameters of the champion cells and average values for PSCs based on perovskite films fabricated with MACl concentrations of 0, 10, and 20 mg/mL.

Sample Code		V_{OC}(V)	J_{SC}(mA cm^{-2})	FF	PCE (%)
MACl-0	Maximum value	1.08	18.90	0.63	12.81
	Average value	1.05	18.43	0.61	11.86
MACl-10	Maximum value	1.09	21.93	0.61	14.56
	Average value	1.08	21.61	0.61	14.27
MACl-20	Maximum value	1.04	22.15	0.58	13.43
	Average value	1.04	21.71	0.56	12.63

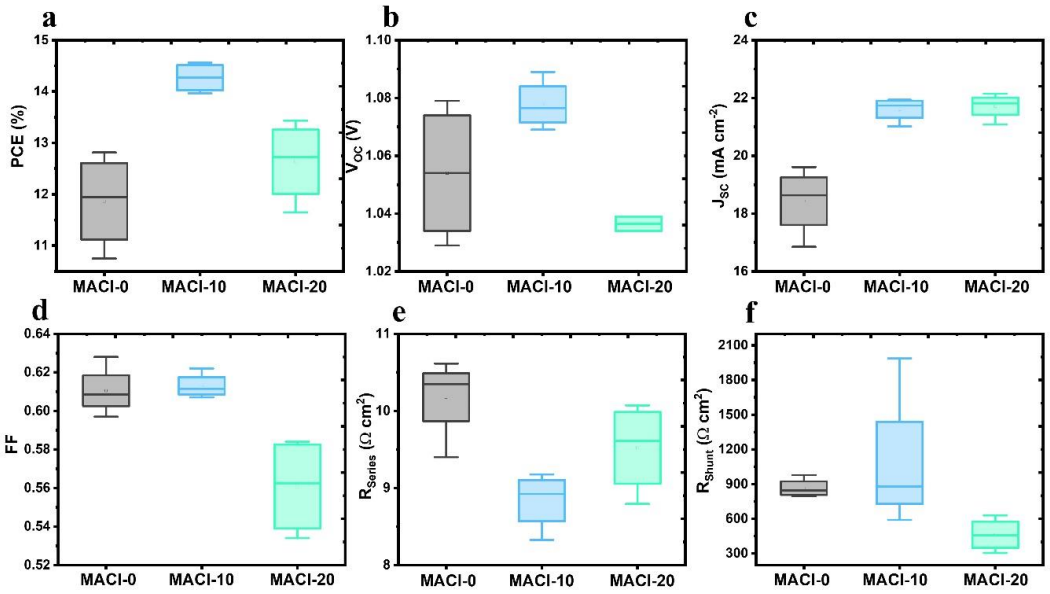

Fig. 4- Statistical distributions of photovoltaic parameters for PSCs fabricated with different concentrations of MACl (0, 10, and 20 mg/mL): (a) PCE, (b) V_{OC}, (c) J_{SC}, (d) FF, (e) R_{Series}, and (f) R_{Shunt}. The experimental parameters are as shown in the caption of Figure 3.

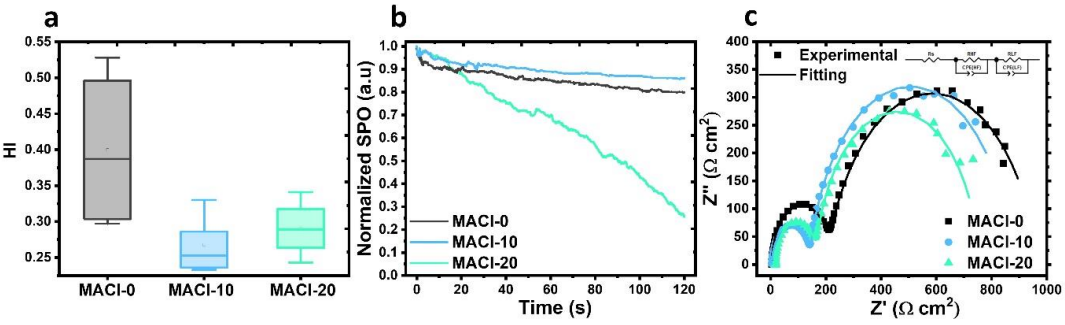

Fig. 5- (a) Statistical distributions of HI; (b) normalized SPO under AM 1.5G illumination at the applied voltage corresponding to the MPP; and (c) Nyquist plots measured under a bias potential of 0.0 V and illumination intensity of 0.1 Sun for PSCs fabricated with different concentrations of MACl (0, 10, and 20 mg/mL).

Table. 2- Fitted parameters extracted from EIS measurements of PSCs fabricated with MACl concentrations of 0, 10, and 20 mg/mL.

	R_s (Ω cm^2)	R_{HF} (Ω cm^2)	C_{HF} (F cm^{-2})	R_{LF} (Ω cm^2)	C_{LF} (F cm^{-2})
MACl - 0	4	203	1.7E-07	760	2.0E-05
MACl - 10	4	138	2.3E-07	773	2.4E-05
MACl - 20	18	147	2.8E-07	590	1.7E-05

In order to more accurately investigate the charge transfer processes and the role of ion migration in the performance of solar cells, electrochemical impedance spectroscopy (EIS) was performed under 0.1 Sun irradiation at a bias voltage of 0.0 V and in the frequency range from 1 MHz to 1 Hz (Figure 5c). The Nyquist plots of all three cells displayed two distinct arcs: the high-frequency (HF) arc is attributed to the charge transfer process, while the low-frequency (LF) arc is associated with electron-hole recombination resistance [29]. The resulting spectra were fitted using an equivalent circuit, shown in the inset in Figure 5c, which includes the external series resistance (Rs) and parallel resistance-constant phase elements (R-CPE) for each arc [30]. The EIS characteristic parameters related to the fitted data are tabulated in Table 2. In the MACl-10 sample, the charge transfer resistance is reduced, indicating a significant improvement in the charge extraction and transfer in the active layers, thereby lowering resistive barriers in the cell structure. Additionally, an increase in the electron-hole recombination resistance is observed in MACl-10 device, indicating reduced non-radiative recombination rate. This phenomenon may be attributed to the suppression of ion migration in the optimal presence of MACl, resulting in greater structural ionic stability under operating conditions. In contrast, the MACl-20 sample shows increased charge transfer resistance and a decreased electron-hole recombination resistance compared to the optimal condition, likely due to the formation of discontinuity regions between grains and an increase in boundary defects. This facilitates ion migration and, as a result, increases non-radiative recombination. These analyses confirm that the optimal MACl incorporation can effectively modulate the ion migration and minimize recombination pathways [27].

4. Conclusions

The findings of this study clearly demonstrate that adding MACl at an appropriate concentration not only enhances the crystallinity of the perovskite layer, but also directly contributes to suppressing non-radiative recombination pathways and reducing ion migration. Specifically, incorporation of MACl at an optimal concentration of 10 mg/mL promotes grain growth and reduces the number of grain boundaries. XRD analysis confirmed an increase in the preferential orientation along the (001) and (002) crystal planes. Furthermore, the efficiency of PSCs with the optimal MACl concentration improved to 14.56%, compared to 12.81% for the control sample. The optimized device showed a significant decrease in the HI, along with lower charge transfer resistance and higher recombination resistance, features that collectively point to more effective charge extraction and better suppression of non-radiative recombination.

References

1. Cao Q, Liu H, Xing J, Li Be, Liu C, Xie F, et al. Optimal methylammounium chloride additive for high-performance perovskite solar cells. Nanomaterials. 2025;15(4):292.
2. Heidariramsheh M, Forouzandeh M, Taghavinia N, Mahdavi SM. Effect of Zn/Sn ratio on perovskite solar cell performance applying off-stoichiometric Cu_2ZnSnS_4/carbon hole-collecting electrodes. ACS Applied Materials & Interfaces. 2022;14(15):17296-311.
3. Zhang L, Wang W, Wei Y, Wang H, Ye J, Lin P, et al. Assessing the effect of excess PbI_2 on the photovoltaic performance of $CsPbI_3$ all-inorganic perovskite solar cells. Materials Today Communications. 2025:112548.
4. Zhou Q, Liu X, Liu Z, Zhu Y, Lu J, Chen Z, et al. Annual research review of perovskite solar cells in 2023. Materials Futures. 2024.
5. Rajabzade S, Abdizadeh K, Mahyari FA, Tajabadi F, Heidariramsheh M, Forouzandeh M, Taghavinia N. Ionic liquid additive in ionic-liquid-based MAPbI3 perovskite ink: Improved film crystallization and device performance in ambient air processed solar cells. Journal of Power Sources. 2025;630:236134.
6. Li S, Dong J, Ji W, Li K, Liu Y, Xu L, et al. Improving efficiency and ultraviolet stability of perovskite solar cells by using multifunctional octocrylene at SnO2 buried interface. Materials Today Communications. 2024;41:111081.
7. Wang H, Zou W, Luo H, Quan Y, Yang L, Liu X, Li H. Ion migration inhibition and defect passivation via sulfonate salt coordination for high-performance perovskite solar cells with enhanced phase stability. Journal of Materials Chemistry C. 2023;11(39):13518-25.
8. Yantara N, Mathews N. Toolsets for assessing ionic migration in halide perovskites. Joule. 2024;8(5):1239-73.
9. Tao J, Zhao C, Wang Z, Chen Y, Zang L, Yang G, et al. Suppressing non-radiative recombination for efficient and stable perovskite solar cells. Energy & Environmental Science. 2025;18(2):509-44.
10. Forouzandeh M, Heidariramsheh M, Heydarnezhad HR, Nikbakht H, Stefanelli M, Vesce L, Taghavinia N. Enhanced carbon-based back contact electrodes for perovskite solar cells: Effect of carbon paste composition on performance and stability. Carbon. 2024;229:119450.
11. Chang J, Feng E, Li H, Ding Y, Long C, Gao Y, et al. Crystallization and orientation modulation enable highly efficient doctor-bladed perovskite solar cells. Nano-micro letters. 2023;15(1):164.
12. Li D, Wu P, Zhang F. Alkylammonium chloride promotes the record efficiency of perovskite solar cells. Joule. 2023;7(4):628-30.
13. Ma D, He J, Sheng J, Shao W, Deng Z, Cen R, et al. Tailoring lattice chlorine in perovskite through dual-additive engineering for enhanced photovoltaic performance. Journal of Materials Chemistry A. 2025;13(2):971-84.
14. Gao H, Zhang M, Xu Z, Chen Y, Hu Y, Yi Z, et al. Low-temperature synergistic effect of MA and Cl towards high-quality α-FAPbI 3 films for humid-air-processed perovskite solar cells. Dalton Transactions. 2024;53(1):136-47.
15. Nandigana P, Saminathan B, Sriram P, Sujatha D, Subramanian B, Panda SK. An ambient process for hole transport layer-free highly stable MAPbI 3 by addition of MACl for efficient perovskite solar cells. Energy Advances. 2024;3(2):442-50.
16. Deng P, Dai W, Gou Y, Zhang W, Xiao Z, He S, et al. Improving thermal stability of high-efficiency methylammonium-free perovskite solar cells via chloride additive engineering. ACS Applied Materials & Interfaces. 2024;16(22):29338-46.
17. Du S, Guo Y, Wang C, Chen G, Li G, Liang J, et al. Improving Crystallization of Wide-Bandgap Lead Halide Perovskite

for All-perovskite Tandems. Advanced Energy Materials. 2025;15(16):2404180.
18. Hassan A, Ke Z, Lin W, Jin Y, Cao Y, Azam M, Xue W. Synergistic effect of additive engineering and ultrafast laser crystallization enabled efficient and stable air-processed perovskite solar cells. Solar Energy Materials and Solar Cells. 2025;287:113614.
19. Yang Z, Niu Y, Zhang X, Zhang Z, Hu L. Efficiency improvement of semi-transparent perovskite solar cells via crystallinity enhancement. Journal of Materials Chemistry A. 2023;11(6):3070-9.
20. Li C, Chowdhury TH, Yoshizawa-Fujita M, Rikukawa M, Yanagida M, Shirai Y, Takeoka Y. Mitigating low-dimensional phases and defects with methylammonium chloride in high-performance Dion–Jacobson quasi-2D tin perovskite solar cells with power conversion efficiency over 6%. Chemical Communications. 2025;61(35):6462-5.
21. Nishimura N, Behera RK, Katoh R, Kanda H, Murakami TN, Matsuzaki H. Unveiled effects of the methylammonium chloride additive on formamidinium lead halide: expediting carrier injection from the photoabsorber to carrier transport layers through spontaneously modulated heterointerfaces in perovskite solar cells. Journal of Materials Chemistry C. 2024;12(25):9130-8.
22. Liu Z, Liu T, Li M, He T, Guo G, Liu P, et al. Eliminating halogen vacancies enables efficient MACL-assisted formamidine perovskite solar cells. Advanced Science. 2024;11(7):2306280.
23. Zhang F, Zhu K. Additive engineering for efficient and stable perovskite solar cells. Advanced Energy Materials. 2020;10(13):1902579.
24. Chen X, Geng C, Yu X, Feng Y, Liang C, Peng Y, Cheng Y-b. Additive engineering in spray enables efficient methylammonium-free wide-bandgap perovskite solar cells. Materials Today Energy. 2023;34:101316.
25. Zou F, Duan C, Zhang Z, Zhu Q, Liu N, Xu S, et al. Grain-boundary passivation by cation reaction minimizes VOC-deficit of 1.8 eV perovskites for efficient all-perovskite tandem solar cells. Nano Energy. 2025;138:110882.
26. Thiesbrummel J, Shah S, Gutierrez-Partida E, Zu F, Peña-Camargo F, Zeiske S, et al. Ion-induced field screening as a dominant factor in perovskite solar cell operational stability. Nature Energy. 2024;9(6):664-76.
27. Zhang Z, Li M, Li R, Zhuang X, Wang C, Shang X, et al. Suppressing ion migration by synergistic engineering of anion and cation toward high-performance inverted perovskite solar cells and modules. Advanced Materials. 2024;36(24):2313860.
28. Luo X, Zhong Y, Gao B, He J, Wang X, Tan L, Chen Y. Dissected MACl Involved Reaction Pathway for Low Temperature Fabrication of High-Efficiency Flexible Perovskite Solar Cells. Angewandte Chemie.e202502949.
29. Ma Q, Zhang Y, Lu C, Zhang R, Wang X, Zhang W, Jiang Z. MACl-induced controlled crystallization in sequentially deposited perovskites for high-efficiency and stable perovskite solar cells. Coatings. 2023;13(11):1885.
30. Ghahremanirad E, Almora O, Suresh S, Drew AA, Chowdhury TH, Uhl AR. Beyond protocols: Understanding the electrical behavior of perovskite solar cells by impedance spectroscopy. Advanced Energy Materials. 2023;13(30):2204370.